Supplement of Atmos. Chem. Phys., 25, 2495–2513, 2025
https://doi.org/10.5194/acp-25-2495-2025-supplement


Atmospheric Chemistry and Physics
Open Access

*Supplement of*

# Measurement report: Cloud condensation nuclei (CCN) activity in the South China Sea from shipborne observations during the summer and winter of 2021 – seasonal variation and anthropogenic influence

**Hengjia Ou et al.**

*Correspondence to:* Mingfu Cai (caimingfu@scies.org)

Section S1, Table S1, Figure S1-S20

**Section S1 CE selection of the Tof-ACSM**

The selection of collection efficiency (CE) was based on previous observation conducted in the South China Sea using the Tof-ACSM (Sun et al., 2023). We primarily considered the influence of two factors: aerosol acidity and the impact of nitrate. The calculation was performed using the following formula (Middlebrook et al., 2012):

Effect of high ammonium nitrate fraction (ANMF):

$$ANMF = \frac{NO_3^- \times \left(\frac{80}{62}\right)}{SO_4^{2-} + NO_3^- + Cl^- + NH_4^+ + Organics} \tag{1}$$

$$CE_{est,ANMF} = 0.0833 + 0.9167 \times ANMF \tag{2}$$

$$CE_{dry,ANMF} = \max\left(0.5, CE_{est,ANMF}\right) \tag{3}$$

Effect of acidity:

$$\frac{NH_4^+{}_{measurd}}{NH_4^+{}_{predicted}} = \frac{NH_4^+/18}{\left(2\times\left(\frac{SO_4^{2-}}{96}\right)+\left(\frac{NO_3^-}{62}\right)+\left(\frac{Cl^-}{35.5}\right)\right)} \tag{4}$$

$$CE_{est,acidity} = 1 - 0.73 \times \left(\frac{NH_4^+{}_{measurd}}{NH_4^+{}_{predicted}}\right) \tag{5}$$

$$CE_{dry,acidity} = \max\left(0.5, CE_{est,acidic}\right) \tag{6}$$

As shown in Fig. S1, the ANNF is higher in winter compared to summer, although the impacts are not highly pronounced. On the other hand, the effect of aerosol acidity is more significant in summer and relatively lower in winter. Taking into account these factors and referring to Crenn et al. (2015), we employed temporal-varying $CE_{dry,acidic}$ according to eq. (6) in this study, as shown in Fig. S3.

In addition, the SMPS data was used to compared with ACSM data in order to verify the CE value. An average particle density (ρ) of 1.5 g cm$^{-3}$ was assumed to convert the PNSD data obtained from the SMPS into mass concentrations (Geller et al., 2006) according to Eq. (7) and Eq. (8):

$$\frac{dV}{dlogDp} = \frac{\pi}{6} D_p^3 \frac{dN}{dlogDp} \tag{7}$$

$$M_{SMPS} = \int_{D_{p,min}}^{D_{p,max}} \rho \frac{dV}{dlogDp} dlogDp \tag{8}$$

where $M_{SMPS}$ is the mass concentration from SMPS, $D_{p,min}$ and $D_{p,max}$ refer to the minimum and maximum particle sizes scanned by the SMPS. dN/dlogDp and dV/dlogDp are particle number size distribution and particle volume size distribution which could be measured by SMPS.

Overall, the mass concentration time series measured by the ACSM and SMPS showed strong correlations, with correlation coefficients of 0.84 and 0.93 for summer and winter, respectively.

However, before May 27 (prior to the onset of the summer monsoon), when air masses predominantly originating from Luzon in the Philippines were observed, SMPS-derived values consistently exceeded those measured by the ACSM. According to Chao et al. (2022), the summer monsoon onset occurred during the sixth pentad of May, which was approximately represented as May 27 for simplicity here. This discrepancy may be attributed to the ACSM's inability to detect certain refractory materials.

To further investigate this discrepancy, we compared black carbon concentrations during two distinct periods, utilizing measurements from the Aethalometer (model AE33). The differences in BC concentration between these periods were minor (0.67 μg m-3 vs 0.48 μg m-3), insufficient to account for the observed discrepancy between the SMPS-derived mass concentration and ACSM mass concentration. It is noteworthy that the AE33 might underestimate BC concentrations during May 5 to 27, owing to the lower detection efficiency for smaller black carbon particles (< 200 nm) relative to larger ones (Nakayama et al., 2010; Drinovec et al., 2015). Prior to May 27, the South China Sea region was predominantly influenced by air masses originating from Luzon. The particle size distribution centered a size range of 50-150 nm (Fig. 2a1 in the manuscript), aligning with the particle size distribution of black carbon from urban emissions reported in Schwarz et al. (2008). It implies that the black carbon might distribute at a relatively small particle size range, which could not fully be detected by the AE33, potentially contributing to the discrepancy between the SMPS-derived and ACSM-measured mass concentrations.

Additionally, we analyzed data from another campaign conducted over the South China Sea in June 2022. During this campaign, a typhoon (Chaba) altered local circulation patterns, leading to the transport of substantial pollutants from the Indochinese Peninsula to the ocean after June 28th (Fig. S19). Under these conditions, the mass concentrations measured by the SMPS were again consistently higher than those measured by the ACSM (Fig. S20), suggesting that the small size black carbon particle could be the primary factor underlying the mass discrepancy.

A review of the literature indicates that discrepancies between SMPS and AMS (or ACSM) measurements have been observed at other locations as well (Sun et al., 2016; Wang et al., 2016; Kuang et al., 2020). When a CE of 0.5 was applied, the correlation coefficient for summer slightly increased from 0.84 to 0.85, though the overall difference remained negligible. Additionally, differences in measurement ranges and methodologies between the SMPS and ACSM are likely contributing factors to these discrepancies.

**Table S1. The $D_{50}$ of different species in external scheme.**

| $D_{50}$ (nm) | 0.1% SS | 0.2% SS | 0.4% SS | 0.7% SS |
|---|---|---|---|---|
| Sulfate | 143 | 90 | 57 | 39 |
| Seasalt | 109 | 69 | 43 | 30 |
| Nitrate | 135 | 85 | 53 | 37 |
| Organic | 242 | 192 | 152 | 126 |

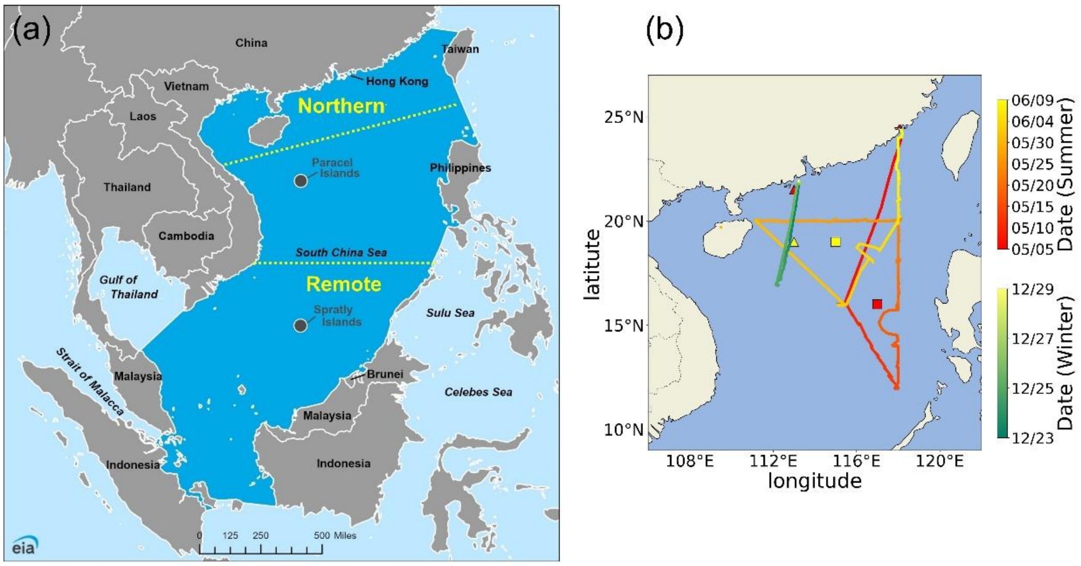


**Figure S1. The definition of South China Sea from U.S. Energy Information Administration (https://www.eia.gov/international/analysis/regions-of-interest/South_China_Sea) and the yellow dash line and text were described the definition of northern and remote South China Sea according to other researches (Atwood et al., 2017; Liang et al., 2021; Zhu et al., 2012) (a); The cruises of these study (b).**

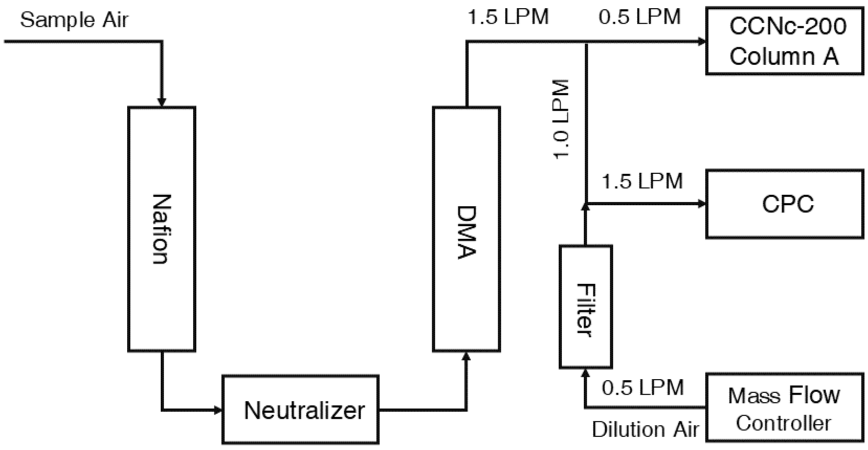


**Figure S2. Instrument setup of the SMCA system.**

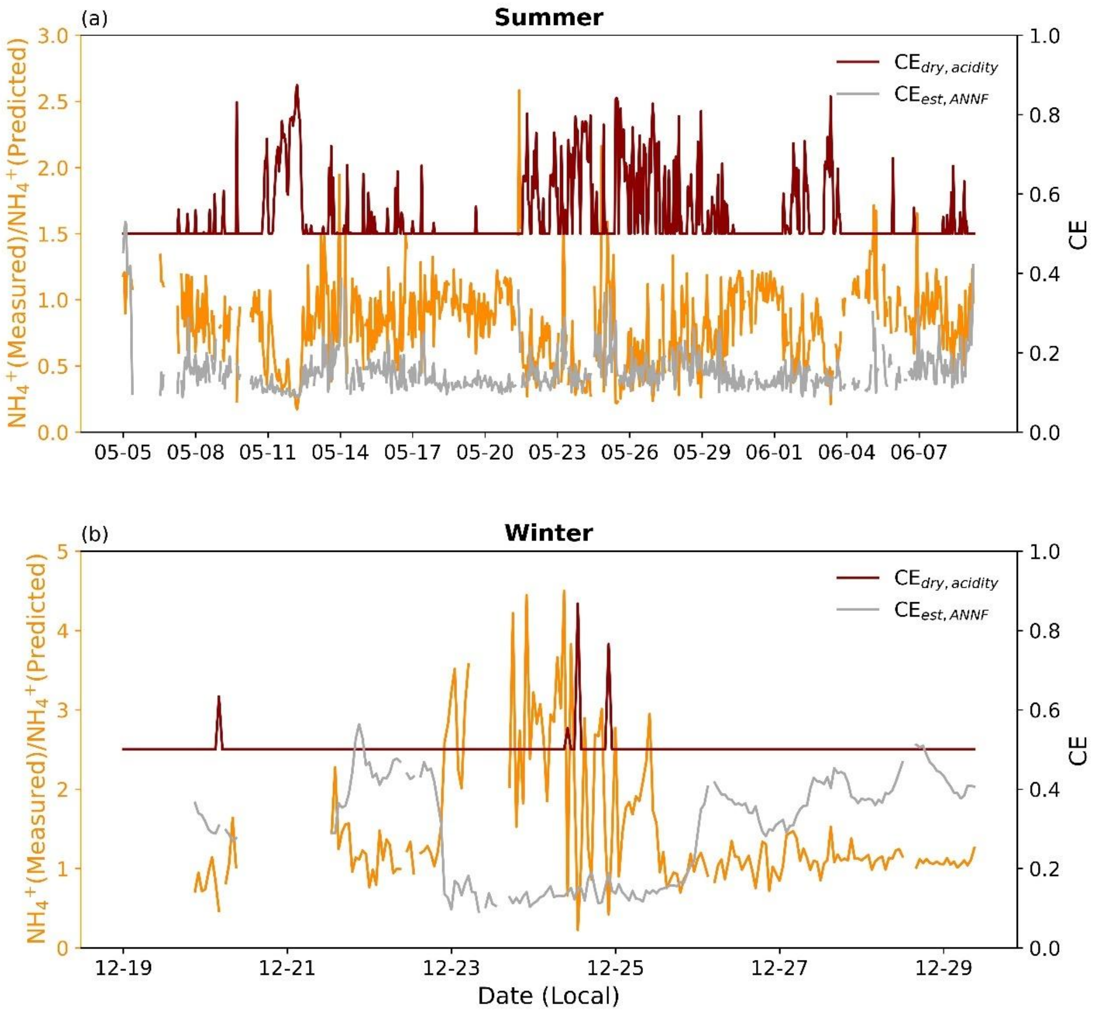


**Figure S3. Timeseries of $CE_{dry,acidity}$, $CE_{est,ANNF}$, and $NH_4^+{}_{,Measured}/NH_4^+{}_{,predicted}$.**

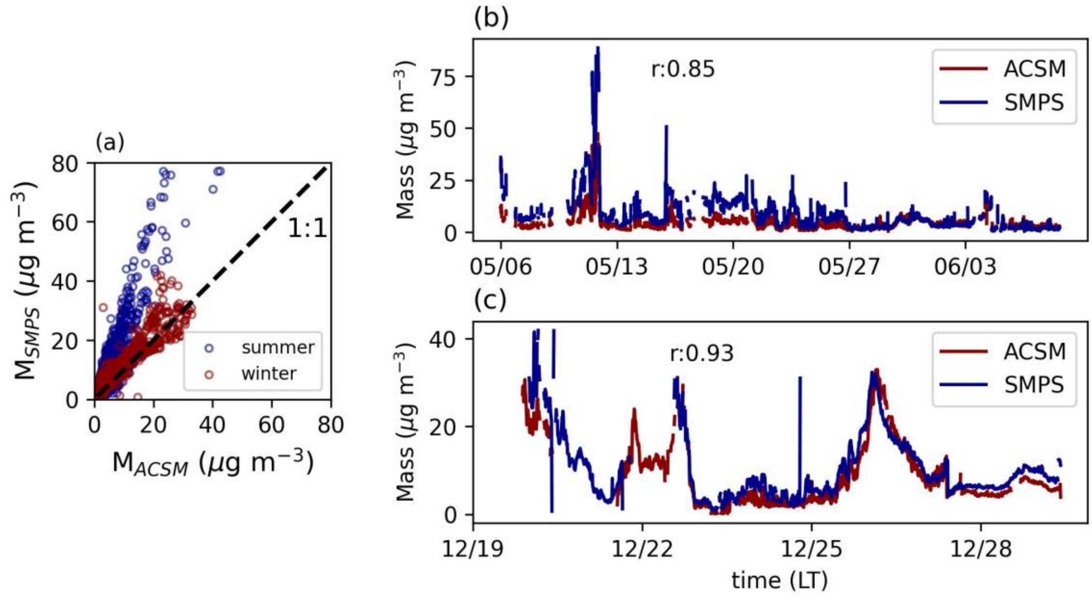


**Figure S4. Comparison of mass concentration from ACSM and SMPS (a), the timeseries of mass concentration of ACSM and SMPS (b).**

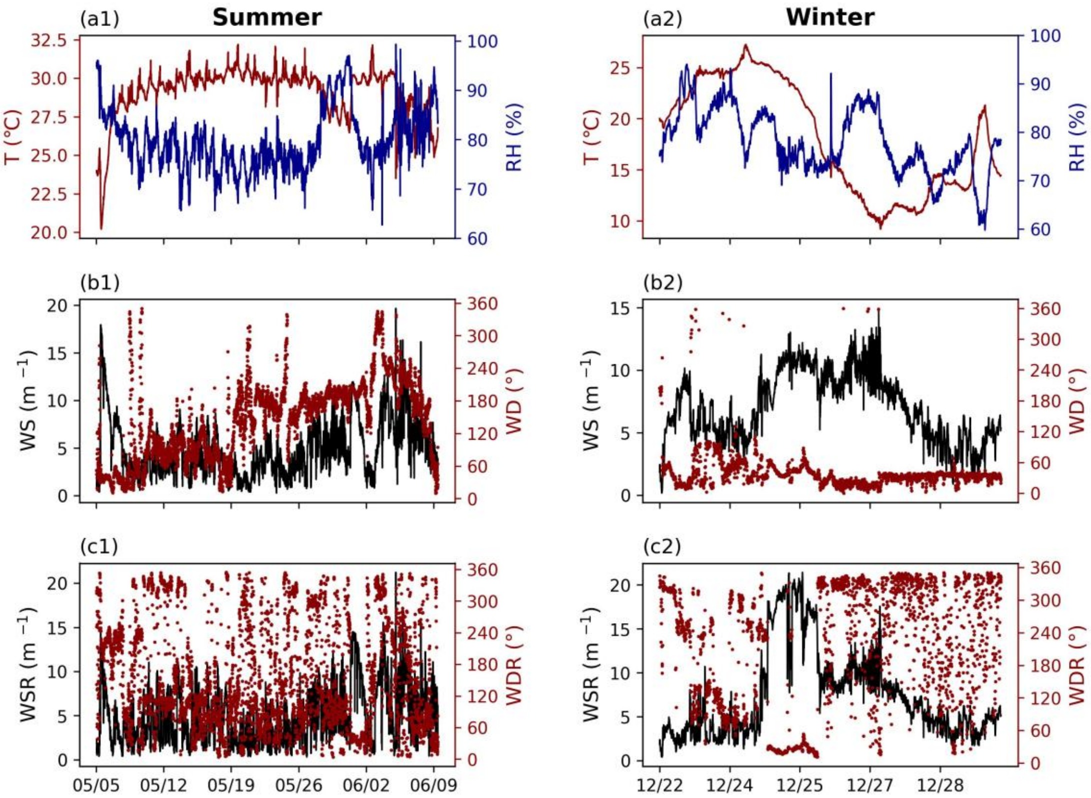


**Figure S5. Timeseries of temperature and relative humility (a), wind speed and wind direction (b), and relative wind speed and relative wind direction (c) in two crusies. The number 1 in figure number is the timeseries in summer and number 2 in figure number is the timeseries in winter.**

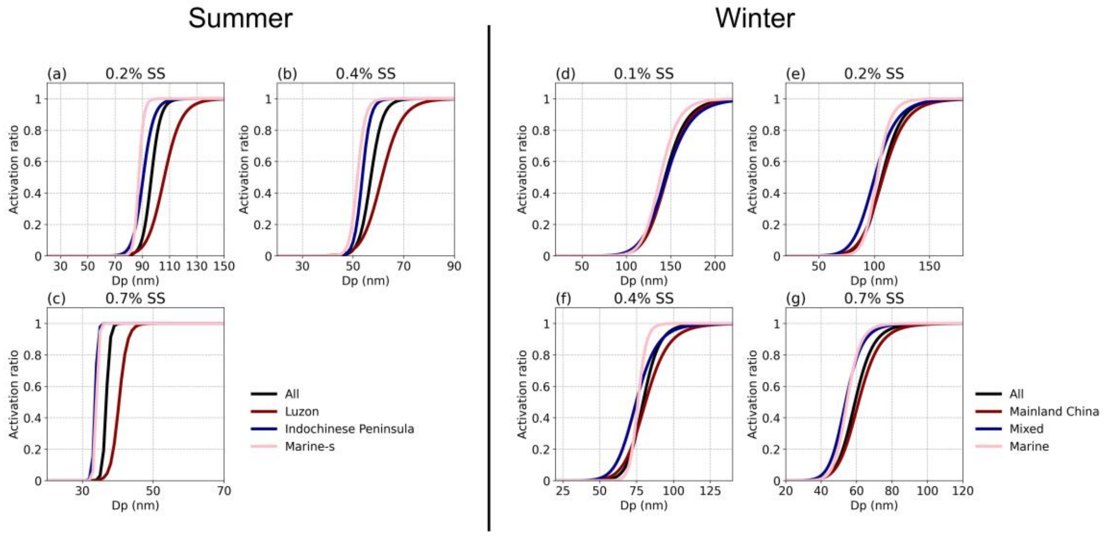


**Figure S6. The average size-resolved activation ratio (AR) fitting result at 0.2% SS (a), 0.4% SS (b), and 0.7% SS (c) in different periods in summer; The average size-resolved activation ratio (AR) fitting result at 0.1% SS (d), 0.2% SS (e), 0.4% SS (f), and 0.7% SS (g) in different periods in winter.**

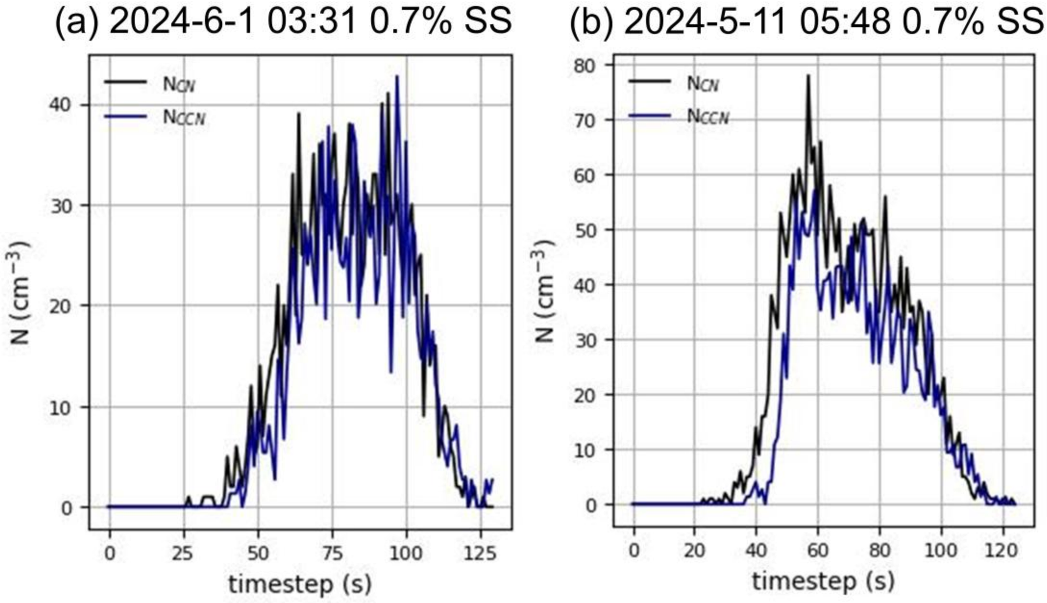


**Figure S7. An example in which D50 cannot be accurately determined (a), and an example in which D50 can be precisely obtained (b).**

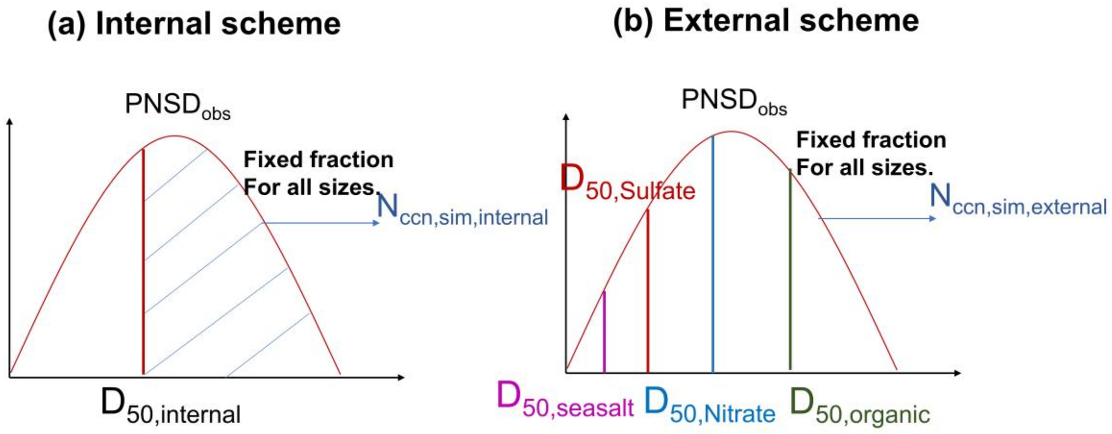


**Figure S8. The internal and external simulation scheme. The D50 in external scheme was shown**

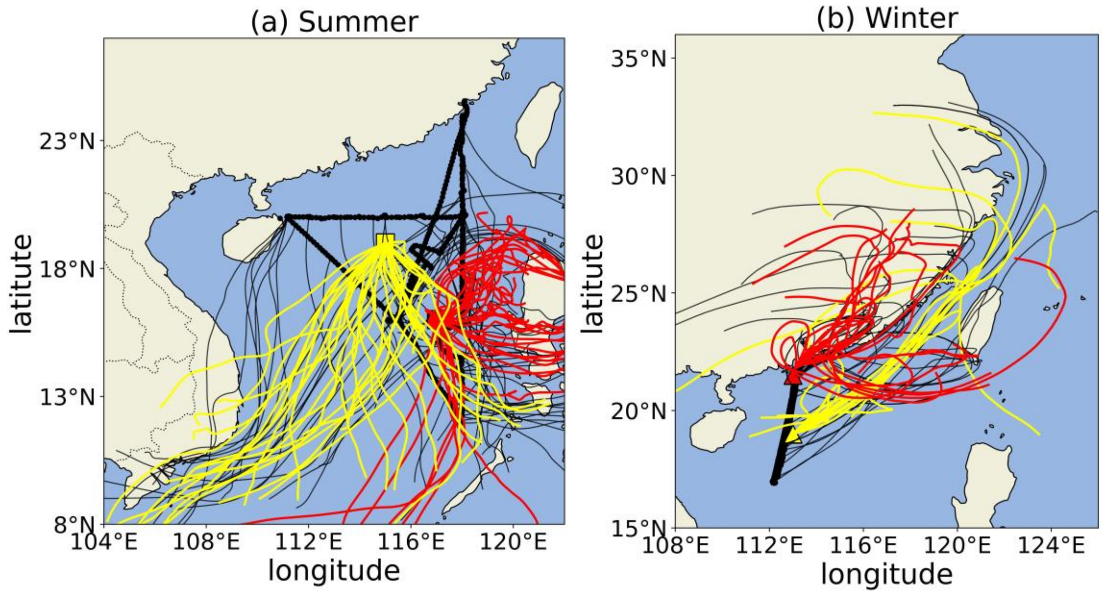


**Figure. S9. The backward trajectories of two midpoints (yellow and red line) and the location of research vessel (black line) during summer cruise (a) and winter cruise (b). The time interval for backward trajectories was 12 hours during the summer. Due to the shorter duration of the winter cruise, the time interval for the winter backward trajectories was set to 6 hours to more accurately distinguish the trajectory sources.**

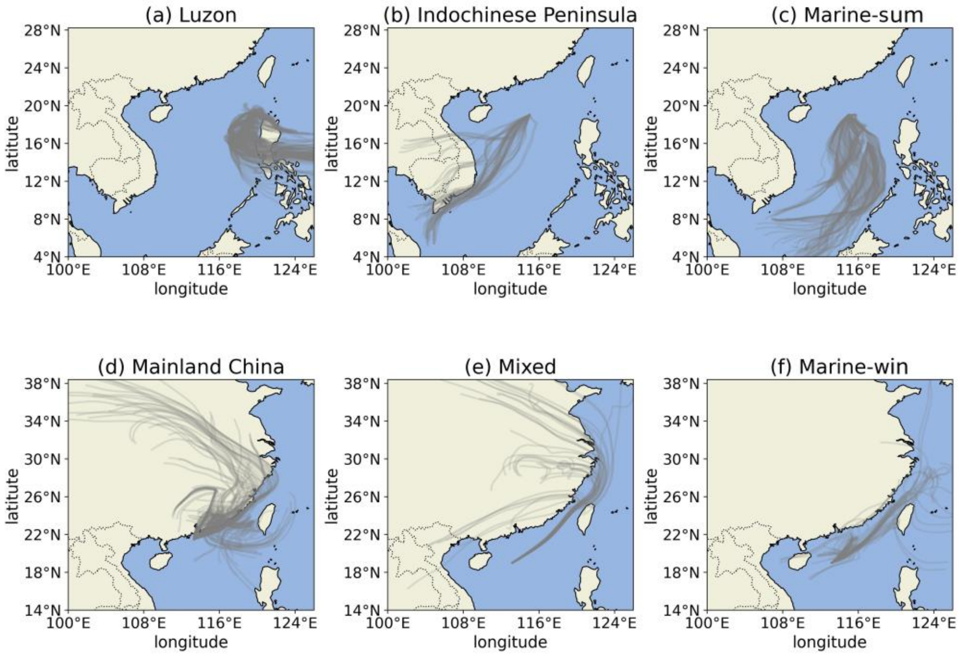


**Figure S10. The backward trajectories of different clusters in summer (a) and winter (b).**

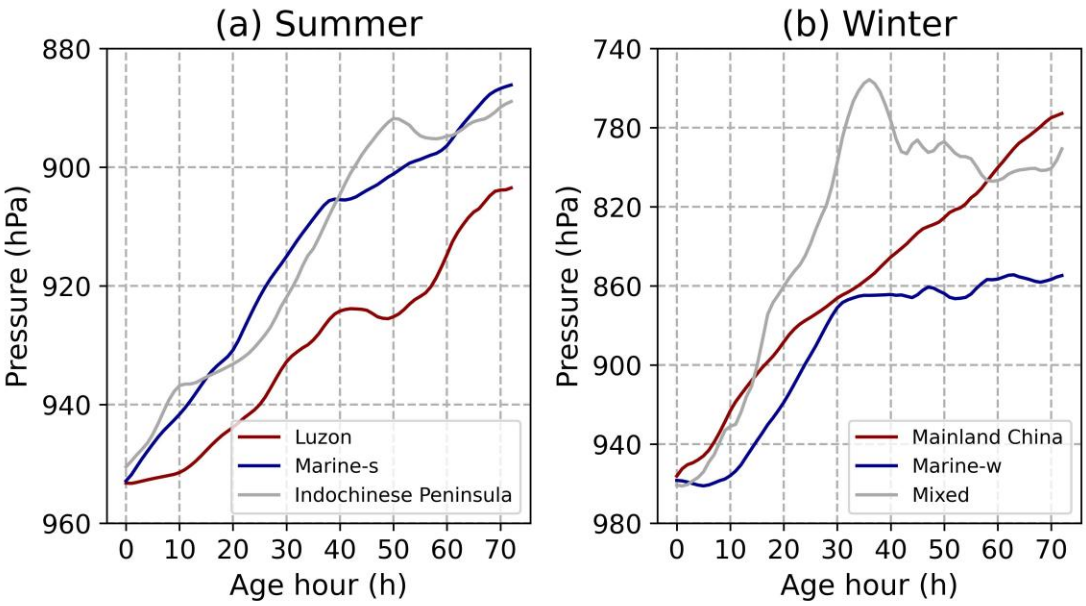


**Figure S11. The average pressure variation as age hour increased in different clusters in summer (a) and winter (b).**

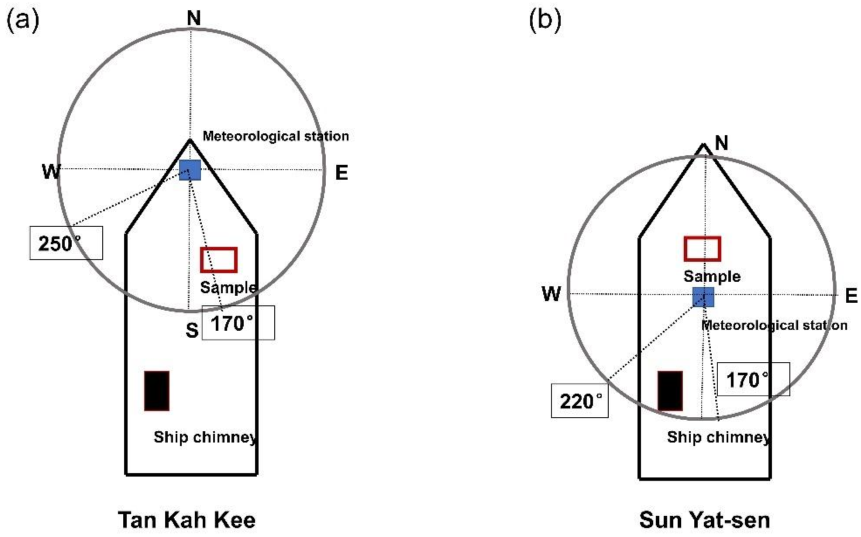


**Figure S12. Instrument and ship chimney loaction in two cruise.**

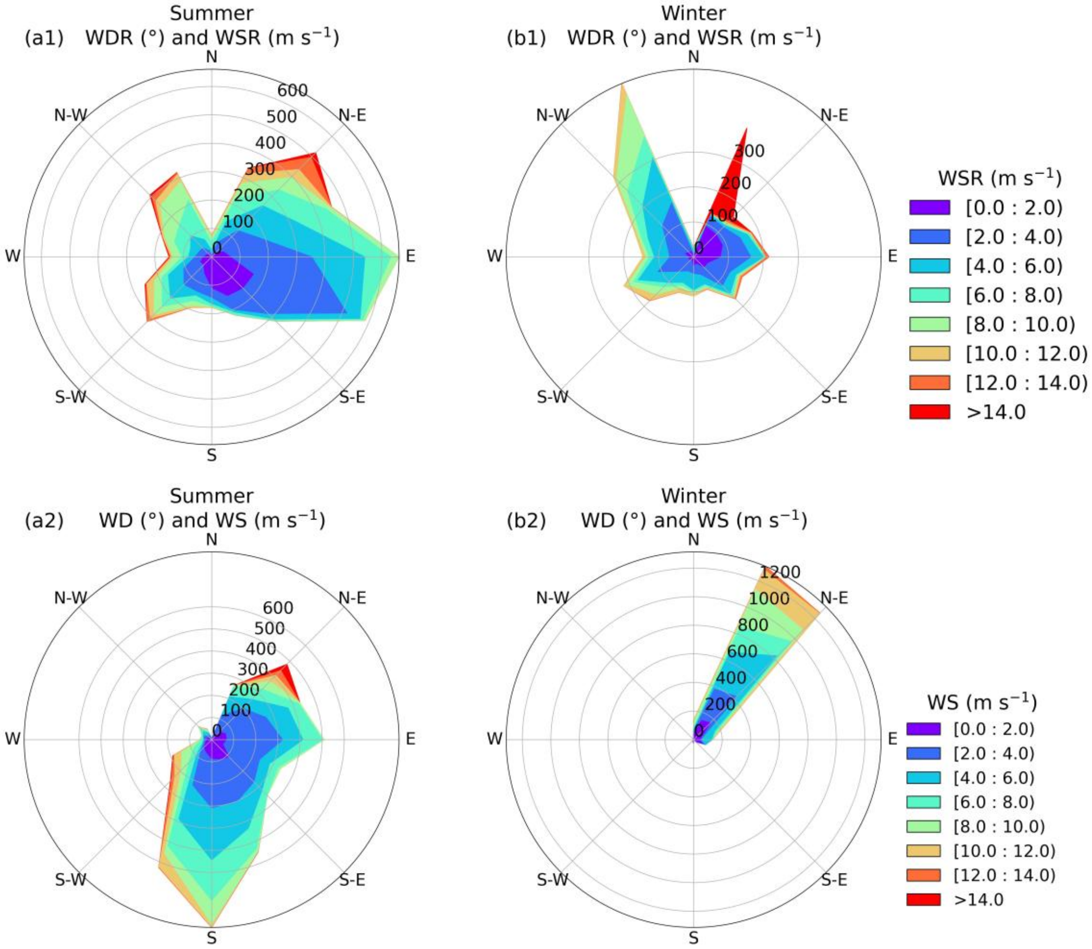


**Figure S13. Wind rose of the relative wind direction (with respect to the bow) and relative wind speed (with respect to the ship speed) in summer and winter cruises; The radius represents the frequency of wind direction occurrences, and the shaded areas indicate wind speed (a1) and (b1); Wind rose of the wind direction and wind speed in summer and winter (a2) and (b2).**

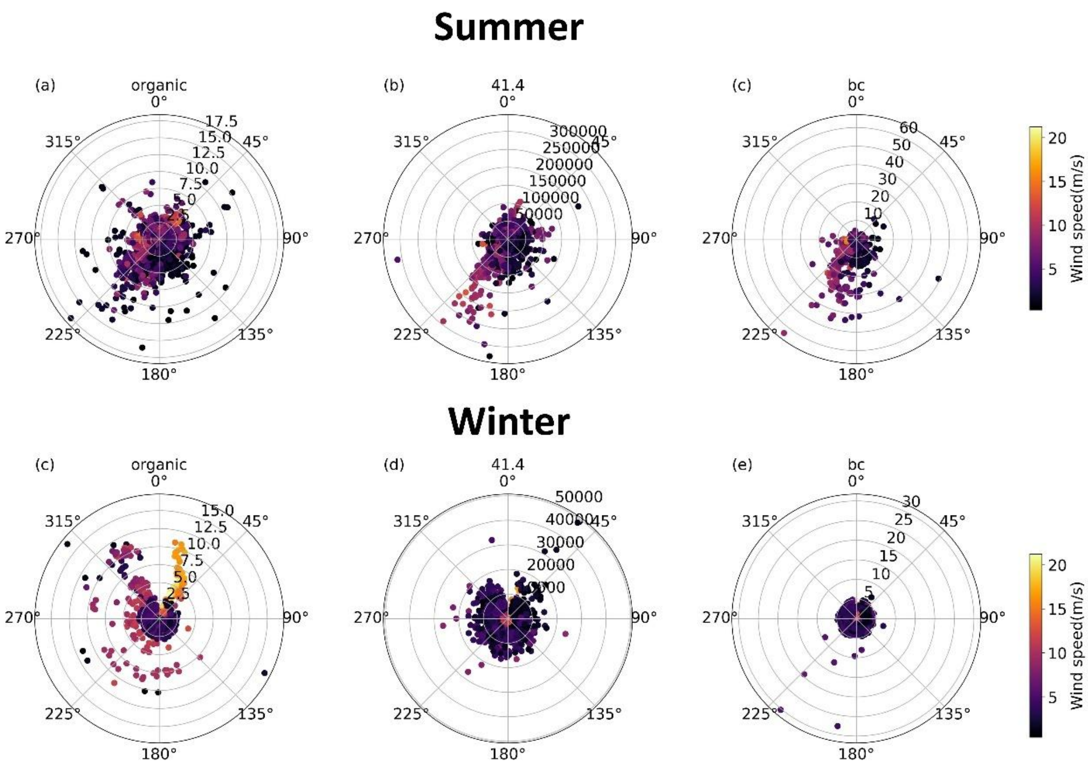


**Figure S14. Wind rose of the organic (μg $m^{-3}$), particle in 41.4 nm ($cm^{-3}$), and black carbon (BC, μg $m^{-3}$) in summer (a-c) and winter (c-e) measurements; The radius represents the organic and BC mass concentration and number concentration (dN/dlogDp) of particle in 41.4 nm, and the color indicate wind speed.**

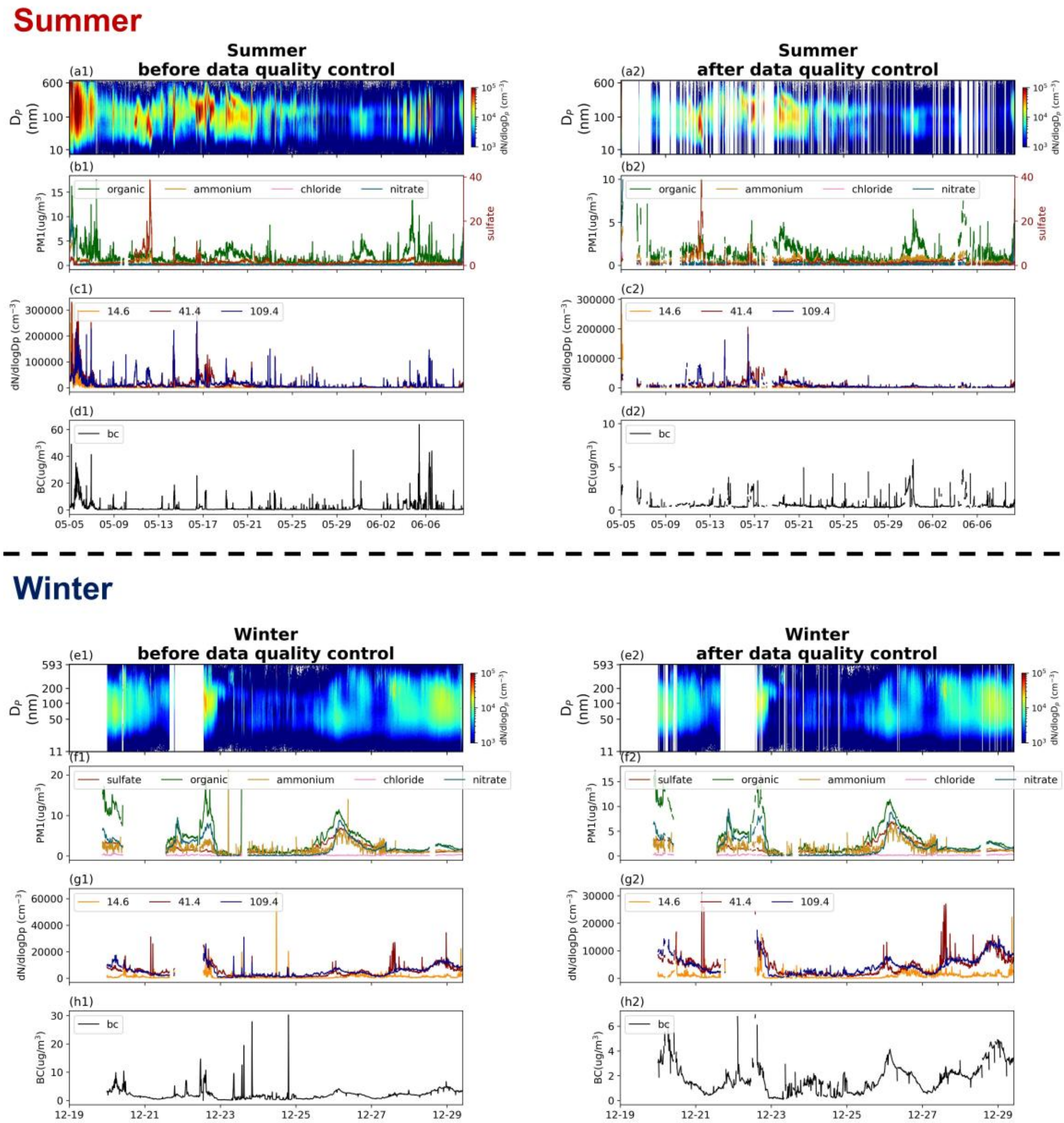


**Figure S15. Timeseries of particle number size distribution (a) and (e), mass concentration of NR-PM$_1$ (b) and (f), particle number concentration in 14.6, 41.4, and 109.4 nm (c) and (g), mass concentration of black carbon (d) and (h); The figure letters from (a) to (d) means the data in summer, and the figure letters from (e) to (h) means the data in winter; The number 1 represented the data before data quality control and the number 2 represent the data after data quality control.**

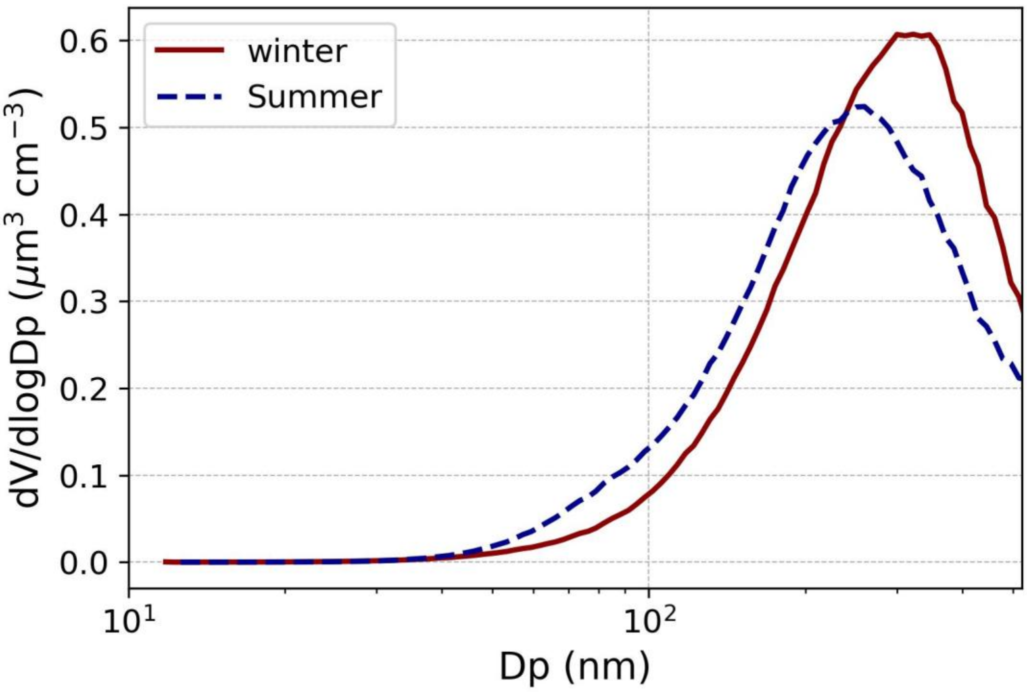


**Figure S16. The average particle volume size distribution during summer and winter.**

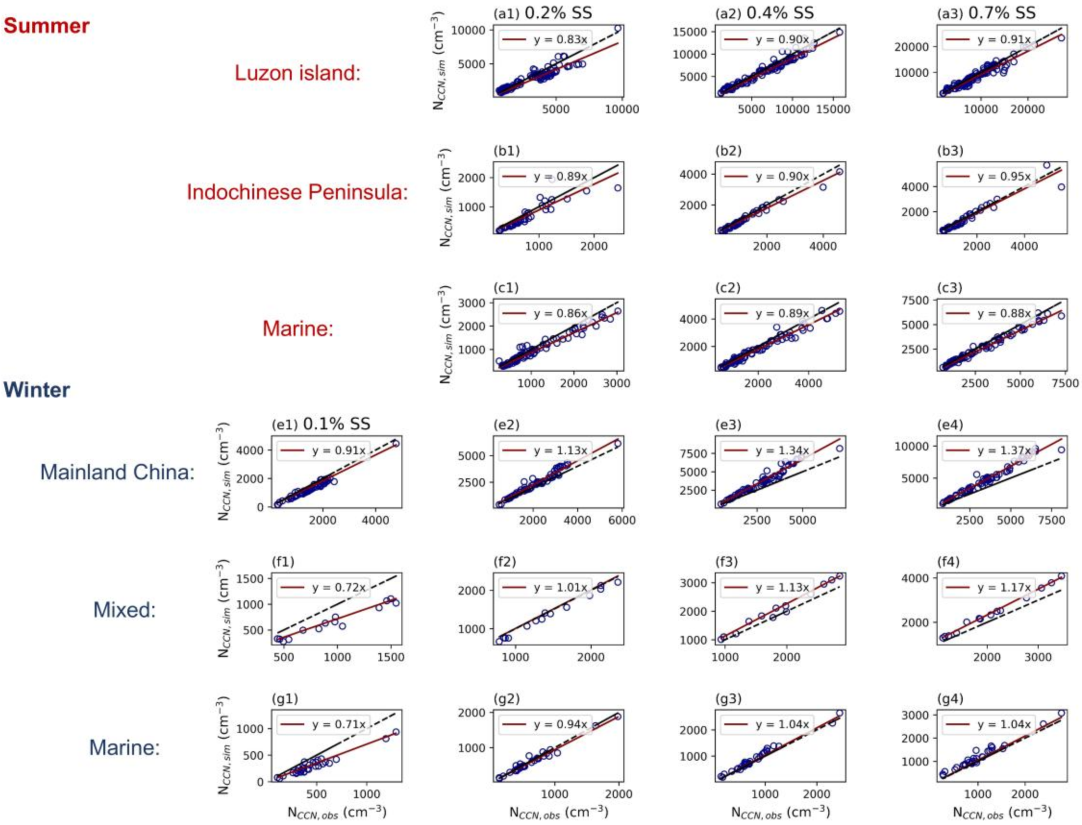


**Figure S17. The fitting result in "Internal-mixed" scheme according to CCN closure method.**

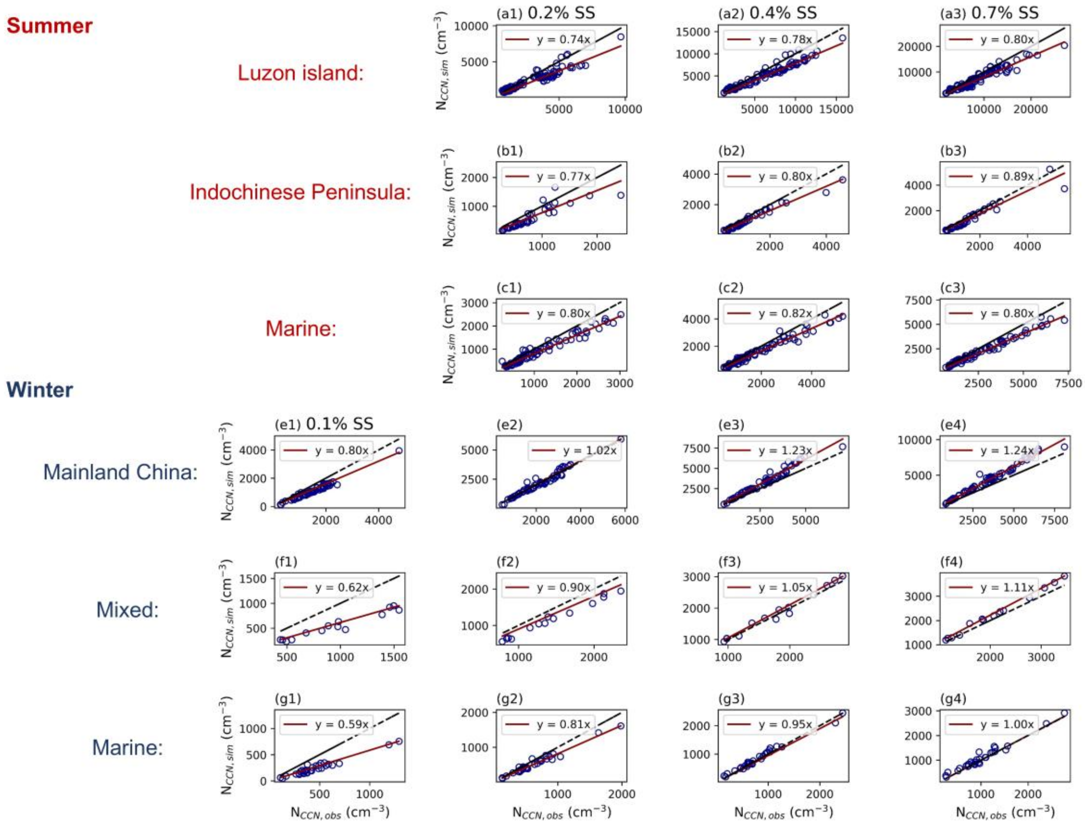


**Figure S18. The fitting result in "External-mixed" scheme according to CCN closure method.**

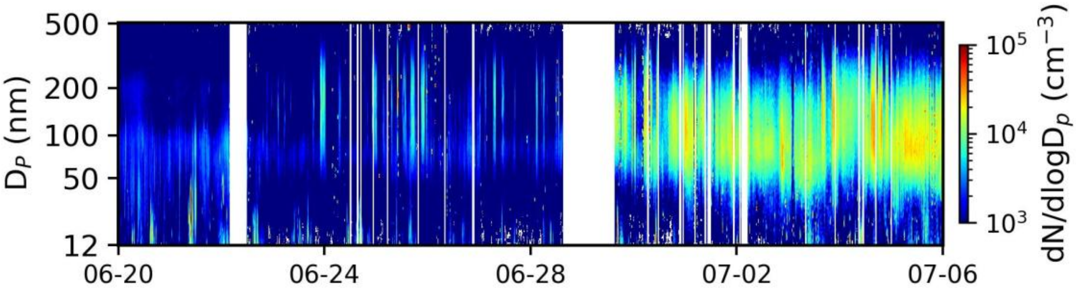


**Figure S19. Timeseries of particle number size distribution in June 2022 in South China Sea.**

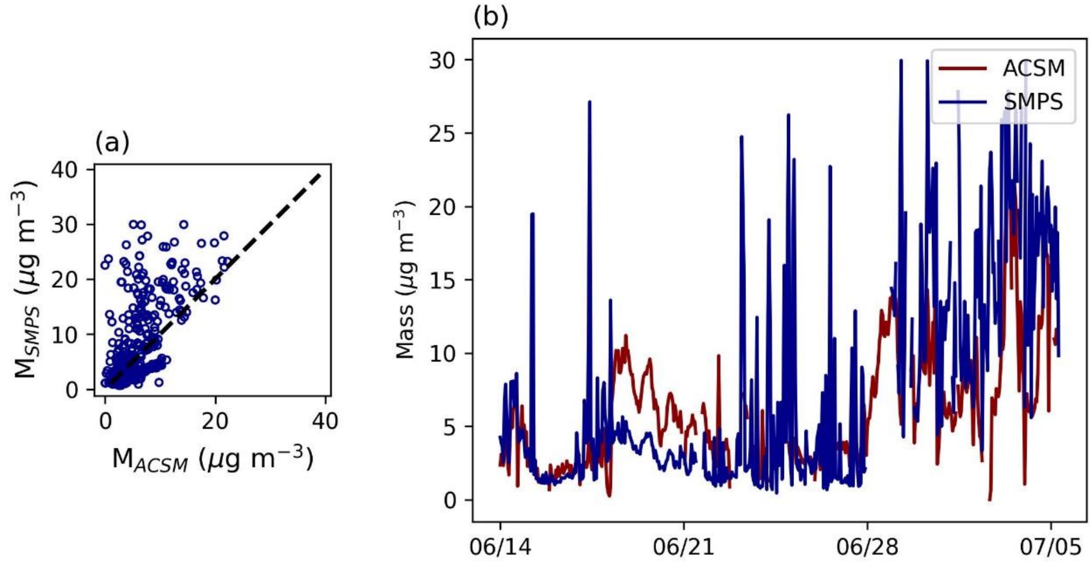


**Figure S20. Comparison of mass concentration from ACSM and SMPS (a), the timeseries of mass concentration of ACSM and SMPS (b).**

## Reference


Atwood, S. A., Reid, J. S., Kreidenweis, S. M., Blake, D. R., Jonsson, H. H., Lagrosas, N. D., Xian, P., Reid, E. A., Sessions, W. R., and Simpas, J. B.: Size-resolved aerosol and cloud condensation nuclei (CCN) properties in the remote marine South China Sea – Part 1: Observations and source classification, Atmos. Chem. Phys., 17, 1105-1123, doi:https://doi.org/10.5194/acp-17-1105-2017, 2017.

Crenn, V., Sciare, J., Croteau, P. L., Verlhac, S., Frohlich, R., Belis, C. A., Aas, W., Aijala, M., Alastuey, A., Artinano, B., Baisnee, D., Bonnaire, N., Bressi, M., Canagaratna, M., Canonaco, F., Carbone, C., Cavalli, F., Coz, E., Cubison, M. J., Esser-Gietl, J. K., Green, D. C., Gros, V., Heikkinen, L., Herrmann, H., Lunder, C., Minguillon, M. C., Mocnik, G., O'Dowd, C. D., Ovadnevaite, J., Petit, J. E., Petralia, E., Poulain, L., Priestman, M., Riffault, V., Ripoll, A., Sarda-Esteve, R., Slowik, J. G., Setyan, A., Wiedensohler, A., Baltensperger, U., Prevot, A. S. H., Jayne, J. T., and Favez, O.: ACTRIS ACSM intercomparison - Part 1: Reproducibility of concentration and fragment results from 13 individual Quadrupole Aerosol Chemical Speciation Monitors (Q-ACSM) and consistency with co-located instruments, Atmos Meas Tech, 8, 5063-5087, doi:https://doi.org/10.5194/amt-8-5063-2015, 2015.

Drinovec, L., Močnik, G., Zotter, P., Prévôt, A.S.H., Ruckstuhl, C., Coz, E., Rupakheti, M., Sciare, J., Müller, T., Wiedensohler, A., Hansen, A.D.A., 2015. The "dual-spot" Aethalometer: an improved measurement of aerosol black carbon with real-time loading compensation. Atmos. Meas. Tech. 8, 1965-1979.

Geller, M., Biswas, S., Sioutas, C., 2006. Determination of Particle Effective Density in Urban Environments with a Differential Mobility Analyzer and Aerosol Particle Mass Analyzer. Aerosol Sci Tech 40, 709-723.

Kuang, Y., He, Y., Xu, W., Zhao, P., Cheng, Y., Zhao, G., Tao, J., Ma, N., Su, H., Zhang, Y., Sun, J., Cheng, P., Yang, W., Zhang, S., Wu, C., Sun, Y., Zhao, C., 2020. Distinct diurnal variation in organic aerosol hygroscopicity and its relationship with oxygenated organic aerosol. Atmos. Chem. Phys. 20, 865-880.

Liang, B., Cai, M., Sun, Q., Zhou, S., and Zhao, J.: Source apportionment of marine atmospheric aerosols in northern South China Sea during summertime 2018, Environmental Pollution, 289, 117948, doi:https://doi.org/10.1016/j.envpol.2021.117948, 2021.

Middlebrook, A. M., Bahreini, R., Jimenez, J. L., and Canagaratna, M. R.: Evaluation of Composition-Dependent Collection Efficiencies for the Aerodyne Aerosol Mass Spectrometer using Field Data, Aerosol Sci Tech, 46, 258-271, doi:https://doi.org/10.1080/02786826.2011.620041, 2012.

Nakayama, T., Kondo, Y., Moteki, N., Sahu, L.K., Kinase, T., Kita, K., Matsumi, Y., 2010. Size-dependent correction factors for absorption measurements using filter-based photometers: PSAP and COSMOS. Journal of Aerosol Science 41, 333-343.

Schwarz, J. P., Gao, R. S., Spackman, J. R., Watts, L. A., Thomson, D. S., Fahey, D. W., Ryerson, T. B., Peischl, J., Holloway, J. S., Trainer, M., Frost, G. J., Baynard, T., Lack, D. A., de Gouw, J. A., Warneke, C., and Del Negro, L. A.: Measurement of the mixing state, mass, and optical size of individual black carbon particles in urban and biomass burning emissions, 35, doi:https://doi.org/https://doi.org/10.1029/2008GL033968, 2008.

Sun, Q., Liang, B., Cai, M., Zhang, Y., Ou, H., Ni, X., Sun, X., Han, B., Deng, X., Zhou, S., and Zhao, J.: Cruise observation of the marine atmosphere and ship emissions in South China Sea: Aerosol composition, sources, and the aging process, Environ. Pollut, 316, 120539, doi:https://doi.org/https://doi.org/10.1016/j.envpol.2022.120539, 2023.

Sun, Y., Jiang, Q., Xu, Y., Ma, Y., Zhang, Y., Liu, X., Li, W., Wang, F., Li, J., Wang, P., Li, Z., 2016. Aerosol characterization over the North China Plain: Haze life cycle and biomass burning impacts in summer. 121, 2508-2521.

Wang, Q., Zhao, J., Du, W., Ana, G., Wang, Z., Sun, L., Wang, Y., Zhang, F., Li, Z., Ye, X., Sun, Y., 2016. Characterization of submicron aerosols at a suburban site in central China. Atmos Environ. 131, 115-123.

Zhu, W., Zhong, K., Li, Y., Xu, Q., and Fang, D.: Characteristics of hydrocarbon accumulation and exploration potential of the northern South China Sea deepwater basins, Chinese Science Bulletin, 57, 3121-3129, doi:https://doi.org/10.1007/s11434-011-4940-y, 2012.